

# 超声振动对激光熔覆高熵合金涂层 组织与耐磨性能的影响

张咪娜<sup>1</sup>, 王以坤<sup>1,2</sup>, 王大锋<sup>3</sup>, 周宇航<sup>1</sup>,  
高世阳<sup>1</sup>, 周述东<sup>1</sup>, 韦超<sup>1</sup>, 李琳<sup>1</sup>

(1.中国科学院宁波材料技术与工程研究所 激光极端制造中心, 浙江 宁波 305201;  
2.宁波大学 材料科学与化学工程学院, 浙江 宁波 315211;  
3.中国兵器科学研究院宁波分院, 浙江 宁波 315103)

**摘要:** **目的** 研究超声振动对高熵合金涂层的裂纹抑制机理与力学性能影响。**方法** 采用自主设计的超声振动平台开展试验。使用激光共聚焦显微镜观察高熵合金涂层的截面形貌, 对比超声添加前后裂纹的数量以及分布情况。采用扫描电镜、X 射线衍射仪等测试设备, 探究添加超声前后涂层的微观组织转变、元素分布趋势与晶粒尺寸等。借助显微硬度仪与往复摩擦磨损试验机研究涂层的显微硬度与耐磨性。**结果** 超声振动作用下, 熔池的润湿角发生变化, 截面由半圆状变为椭圆状。超声振动显著细化涂层的晶粒, 破碎的柱状晶增加了凝固晶核的数量, 同时促进了 FCC 相在晶界处的析出。FCC 析出相形成“网状”结构, 增强了晶界处吸收应力的能力, 有助于抑制涂层中裂纹的扩展。涂层显微硬度由 503HV0.5 提升至 526HV0.5, 室温摩擦因数由 0.669 下降至 0.586, 摩擦曲线更加平稳。添加超声振动后, 涂层的磨损机制为磨粒磨损与氧化磨损。**结论** 超声振动产生的空化效应与声流效应减小了熔池的温度梯度, 细化了晶粒, 抑制了裂纹在晶界处扩展。添加超声振动后, 涂层的力学性能与摩擦性能得到提升。

**关键词:** 超声振动; 高熵合金; 激光熔覆; 裂纹抑制; 微观组织; 耐磨性能

中图分类号: TG174.44 文献标志码: A 文章编号: 1001-3660(2024)13-0022-11

DOI: 10.16490/j.cnki.issn.1001-3660.2024.13.003

## Effect of Ultrasonic Vibration on Organization and Wear Resistance of Laser Cladding High Entropy Alloy Coatings

ZHANG Mina<sup>1</sup>, WANG Yishen<sup>1,2</sup>, WANG Dafeng<sup>3</sup>, ZHOU Yuhang<sup>1</sup>,  
GAO Shiyang<sup>1</sup>, ZHOU Shudong<sup>1</sup>, WEI Chao<sup>1</sup>, LI Lin<sup>1</sup>

(1. Research Centre for Laser Extreme Manufacturing, Ningbo Institute of Materials Technology & Engineering,  
Chinese Academy of Sciences, Zhejiang Ningbo 305201, China;

收稿日期: 2024-04-26; 修订日期: 2024-06-03

Received: 2024-04-26; Revised: 2024-06-03

**基金项目:** 国家重点研发计划项目 (2023YFB4607000); 浙江省重点研发计划项目 (2024C01178); 中国科学院宁波材料技术与工程研究所所长基金 (E30902QF14); 中国兵器工业集团第五二研究所所列基金 (NBFJ2022-07); 中国兵器工业集团第五二研究所优秀青年科技人才培养基金项目 (YQJJ2023-04)

**Fund:** National Key R&D Program of China (2023YFB4607000); Key Research and Development Program of Zhejiang Province (2023Z098); Director's Fund of Ningbo Institute of Materials Technology and Engineering, Chinese Academy of Sciences (E30902QF14); Foundation of No.52 Research Institute of China Ordnance Industry (NBFJ2022-07); The No.52 Research Institute of China Ordnance Industry Fund for Outstanding Young Scholars (YQJJ2023-04)

**引文格式:** 张咪娜, 王以坤, 王大锋, 等. 超声振动对激光熔覆高熵合金涂层组织与耐磨性能的影响[J]. 表面技术, 2024, 53(13): 22-32.  
ZHANG Mina, WANG Yishen, WANG Dafeng, et al. Effect of Ultrasonic Vibration on Organization and Wear Resistance of Laser Cladding High Entropy Alloy Coatings[J]. Surface Technology, 2024, 53(13): 22-32.

2. School of Materials Science and Chemical Engineering, Ningbo University, Zhejiang Ningbo 315211, China;

3. Ningbo Branch of Chinese Academy of Ordnance Science, Zhejiang Ningbo, 315103, China)

**ABSTRACT:** High entropy alloys (HEA) is a type of multi-major element alloys composed of various metal elements. Among many HEA systems, dual-phase HEAs (such as AlCoCuFeNi, AlCoCrCuFeNi, and CrCuFeMnNi, etc.) can combine strength and toughness perfectly under specific conditions. They possess good ductility, oxidation, wear, and corrosion resistance, making them excellent choices for the preparation of protective coating materials for metals. The excellent choices for protective coating materials include the following methods: magnetron sputtering, electrochemical deposition, arc melting, and laser melting. Laser cladding technology offers advantages such as a low dilution rate, strong metallurgical bonding, good densification, and controllable thickness. However, differences in melting points of many elements in high-entropy alloys, and different solidification sequences, can lead to porosity. Moreover, the rapid solidification effect can produce large local residual stresses, potentially resulting in cracks. Therefore, the coating technology of high-entropy alloys prepared by laser melting and cladding needs further optimization. In recent years, researchers have found that ultrasonic vibration, as an external energy field, can decrease the defects in laser cladding technology and regulate the organization and properties of the cladding layer. The cavitation effect, acoustic flow effect, and thermal effect induced by ultrasonic vibration have a positive influence on the solidification process of metal melt, which can alter the flow mode of the melt, reduce the temperature gradient, refine the grain, and inhibit segregation. The work aims to investigate the effect of ultrasonic vibration on the solidification process of metal melt and to explore its impact on mechanical properties, particularly the inhibition of crack formation in high-entropy alloy coatings.

A self-designed ultrasonic vibration platform with a vibration frequency of 20.1 kHz was used to conduct the experiment. The vibration of the platform was measured by a laser vibrometer, and the ultrasonic amplitude generated by the platform ranged from 1.5 to 9.5  $\mu\text{m}$ . After preliminary exploration and process optimization, an ultrasonic amplitude of 5  $\mu\text{m}$  was selected. 304 stainless steel was used as the coated substrate, and the particle size range of the AlCoCuFeNi high-entropy alloy powder was 53  $\mu\text{m}$ . The particle size of the AlCoCuFeNi high-entropy alloy ranged from 53 to 150  $\mu\text{m}$ . The laser power used for the coating test was 900 W, with a scanning speed of 7 mm/s. At the conclusion of the test, the cross-sectional morphology of the high-entropy alloy coatings was observed with a laser confocal microscope to compare the number and distribution of cracks before and after the addition of ultrasonic vibration. A scanning electron microscopy, an X-ray diffractometry, and other testing equipment were utilized to characterize the microstructural transformation of the coating before and after ultrasonic treatment, including trends in element distribution and grain size. The microhardness and wear resistance of the coatings were examined with a microhardness tester and a reciprocating friction and wear tester.

Under the influence of ultrasonic vibration, the macroscopic morphology of the coating changed. High-frequency vibration reduced the contact angle between the molten pool and the substrate, causing the coating cross section to change from semicircular to elliptical. In the original coating, cracks ran through the coating at the overlap joints; however, after the addition of ultrasonic vibration, the coating exhibited improved continuity and metallurgical bonding at the overlap joints. The acoustic flow effect generated by ultrasonic vibration altered the flow pattern of the melt pool, while the stirring effect reduced the temperature gradient and suppressed the formation of dense dendritic crystals at the root of the coating. The micro-shock waves generated by cavitation and the instantaneous high temperature interrupted the columnar crystals inside the coating, leading to significant grain refinement. The change in the temperature gradient of the molten pool and the grain refinement increased the precipitation of FCC phase, which was distributed in the form of a "mesh" at the overlap joints of the coatings, inhibiting crack extension. Consequently, the mechanical properties of the coatings were improved by ultrasonic vibration. The average microhardness increased from 503HV0.5 to 526HV0.5, and the coefficient of friction decreased, with reduced fluctuation in the curve. The coefficient of friction decreased from 0.669 to 0.586, the catalytic cracking precipitation phase induced by ultrasonic vibration reduced the formation of microcracks in the coating during the friction process, the grain refinement led to improved friction performance, and the wear mechanism was abrasive wear with slight oxidative wear.

**KEY WORDS:** ultrasonic vibration; high entropy alloys; laser cladding; crack suppression; microstructure; wear resistance

高熵合金 (HEAs) 是由多种金属元素构成的一种多主元合金,不同元素的晶体结构与化学位存在差异,使得高熵合金具有高熵效应、迟滞扩散效应、晶格畸变效应与鸡尾酒效应<sup>[1-2]</sup>。研究人员可以通过改变元素的含量调控高熵合金的结构与性能,从而实现理想性能合金的高效设计与制备<sup>[3-4]</sup>。在众多高熵合金体系中,AlCoCrCuFeNi 系高熵合金具有 BCC+FCC 的双相结构,Al 元素是 BCC 相稳定元素,Cu 又促进了 FCC 相的形成。与单相 HEAs 相比,双相 HEAs (如 AlCoCuFeNi、AlCoCrCuFeNi 和 CrCuFeMnNi 等)可以将强度和韧性在特定条件下完美结合,具有良好的延展性和抗氧化性、耐磨性和耐腐蚀性<sup>[5-8]</sup>,是金属保护涂层材料的优良选择。

制备高熵合金涂层的方法主要有以下几种:磁控溅射<sup>[9]</sup>、电化学沉积<sup>[10]</sup>、电弧熔覆<sup>[11]</sup>与激光熔覆<sup>[12]</sup>等。激光熔覆技术具有稀释率低、冶金结合力强、致密性好、厚度可控等优点<sup>[13]</sup>。但是,激光熔覆技术过程中,金属粉末发生瞬间的熔化与凝固,熔池的局部抖动、粉末间隙与低熔点物质的蒸发均会在凝固过程中引发气孔<sup>[14]</sup>,快速凝固效应也会产生较大的局部残余应力,引发裂纹<sup>[15]</sup>。因此,激光熔覆制备高熵合金涂层技术亟须优化。

近年来,研究人员发现,超声振动作为外部能场,可以改善激光熔覆技术中出现的缺陷,调控熔覆层的组织与性能<sup>[16]</sup>。Wang 等<sup>[17]</sup>在激光熔覆陶瓷相增强铁基合金涂层的过程中添加了超声振动,发现超声振动不仅减少了涂层上方的未熔黏粉数量,而且涂层表面更加光滑;另一方面,超声振动的引入细化了大块的陶瓷相颗粒,涂层的显微硬度与摩擦性能得到提升。超声振动引发的空化效应、声流效应与热效应协同作用对金属熔体的凝固过程有着积极的影响,可以改变熔体的流动方式<sup>[18]</sup>、减小温度梯度<sup>[19]</sup>、细化晶粒<sup>[20]</sup>与抑制偏析<sup>[21]</sup>等。Wang 等<sup>[22]</sup>利用 X 射线同步辐射揭示了原位超声振动辅助制备铋基合金的内部变化,发现超声振动产生的空化泡会根据声压的大小发生空化效应,瞬态空化时产生的微冲击波能迅速打破正在

凝固的晶粒。Ji 等<sup>[23]</sup>将超声振动耦合到激光熔覆的有限元模型中,发现超声振动可以提升减小熔池的润湿角,同时提升熔池内部环流的速度,进而减小熔池内部的温度梯度。目前诸多关于超声振动辅助激光熔覆的研究主要集中于常见合金,如 Fe 基、Ni 基与 Co 基合金等,关于超声振动调控高熵合金涂层组织与性能的研究较少;另外,利用超声振动改善激光熔覆高熵合金搭接裂纹的方法较为少见。基于此,本文采用超声振动辅助激光熔覆的方法,在 304 不锈钢上制备了 AlCoCuFeNi 高熵合金涂层,着重研究了超声振动对高熵合金涂层的裂纹抑制、显微硬度与摩擦性能的影响,对超声振动辅助激光熔覆高熵合金涂层的应用起到一定的指导作用。

## 1 试验

### 1.1 熔覆基板与材料

本文的试验采用 304 不锈钢作为熔覆基板,化学成分如表 1 所示。基板尺寸为 250 mm×150 mm×12 mm。进行激光熔覆试验前,用 1000#砂纸将基板表面打磨光滑,去除表面的杂质,随后使用酒精清洗基板表面,待酒精挥发后备用。熔覆使用的 AlCoCuFeNi 高熵合金粉末采用北京研邦新材料科技有限公司的气雾化合金粉末,粒度范围为 53~150  $\mu\text{m}$ ,粉末的微观形貌与元素分布如图 1 所示。粉末的球形度较好,粒度均匀,仅存在少量行星状黏粉。EDS 结果表明,Al、Co、Cu、Fe、Ni 等 5 种元素在粉末中分布均匀。正式试验前,将高熵合金粉末放入 DZF 型真空干燥箱,在 80  $^{\circ}\text{C}$  下恒温烘干 3 h,随后取出备用。

表 1 304 不锈钢基板的化学成分  
Tab.1 Chemical composition of 304 stainless steel substrate

wt.%								
C	Si	Mn	P	S	Cr	Ni	N	Fe
0.054	0.325	0.764	0.038	0.007	18.100	8.020	0.689	Bal.

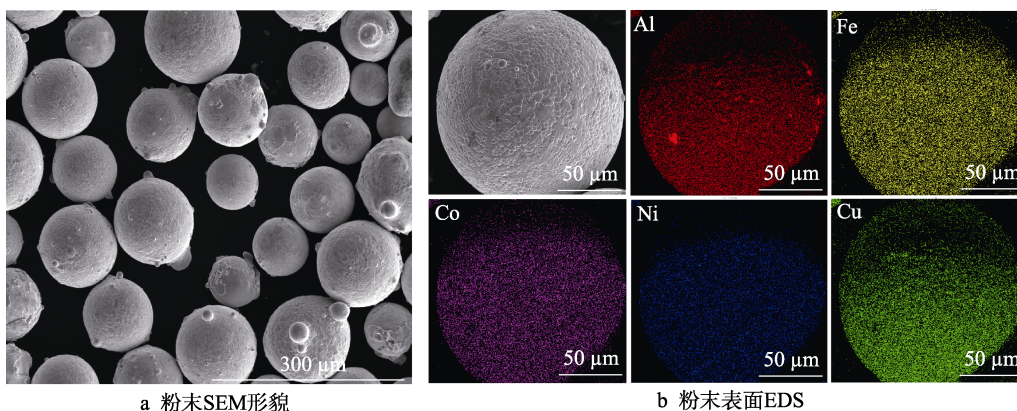


图 1 AlCoCuFeNi 高熵合金粉末微观形貌与元素分布

Fig.1 Micro-morphology and elemental distribution of AlCoCuFeNi high-entropy alloy powder

1.2 设备与方案

超声振动辅助激光熔覆试验系统如图 2 所示。主要包括激光器 (Rofin FL 040, 德国)、机械臂 (KUKA KR-60, 德国)、同轴送粉器 (RC-PGF-D-2, 中国)、试验平台与冷却水循环机等。试验采用高纯度的氩气作为保护气与送粉气体, 防止熔覆层凝固后表面氧化。超声振动通过自主设计的底部超声振动装置产生, 该装置的振动频率为 20 kHz, 利用激光测振仪测量振动平台的振动情况, 平台产生的超声振幅范围为 1.5~9.5  $\mu\text{m}$ 。经过前期的探索与工艺优化, 选定超声振幅为 5  $\mu\text{m}$ 。激光熔覆采用的光斑为直径 2 mm 的圆形光斑, 激光功率为 900 W, 光斑移动速度为 7 mm/s, 熔覆道之间的搭接率为 30%。具体试验参数如表 2 所示。

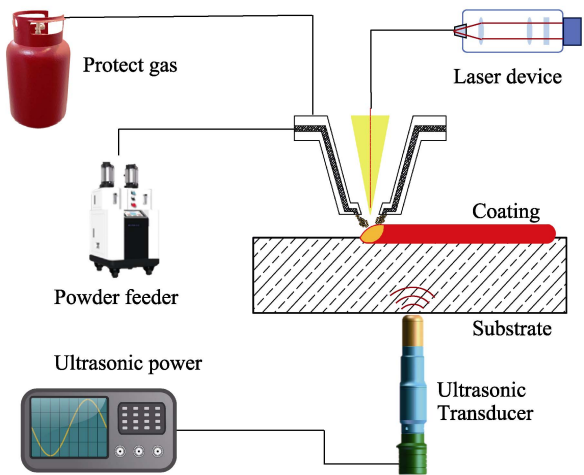


图 2 超声辅助激光熔覆系统  
Fig.2 Ultrasonic-assisted laser cladding systems

表 2 激光熔覆试验工艺参数  
Tab.2 Laser cladding test process parameters

Laser power/ W	Scanningspeed/ (mm·s <sup>-1</sup> )	Overlap/%	Powder gas/ (L·min <sup>-1</sup> )	Shield gas/ (L·min <sup>-1</sup> )	Ultrasonic frequency/kHz	Ultrasonic amplitude/ $\mu\text{m}$	Laser spot diameter/mm
900	7	30	7.5	15	20	5	2

熔覆试验结束后, 使用体视镜拍摄熔覆层表面成形情况, 随后使用数控电火花线切割机进行取样, 取样方向为垂直于激光熔覆方向。使用 X 射线衍射仪 (D8 ADVANCE) 分析涂层表面的物相, 采用 Cu-K $\alpha$  射线源, 扫描角度范围为 20°~90°, 速率为 8 (°)/min。随后将样品镶嵌, 分别使用 200<sup>#</sup>、500<sup>#</sup>、1000<sup>#</sup>、1500<sup>#</sup>、2000<sup>#</sup>和 5000<sup>#</sup>的砂纸进行研磨, 研磨后采用金刚石与 SiO<sub>2</sub> 悬浮液进行精细抛光。抛光结束后, 用共聚焦显微镜 (VK-X200K) 进行截面形貌观察, 随后使用配有 X 射线能谱仪 (EDS) 的扫描电子显微镜 (SEM Quanta 250 FEG) 观察截面的微观组织与元素分布。使用电子探针 (EPMA JXA-iHP200F) 检测搭接裂纹处的元素分布。将样品进行振动抛光后, 使用电子背散射仪 (EBSD Verios G4 UC) 统计涂层内部的晶粒尺寸、晶体取向与相分布。

使用 RDHVS-1000Zmicro 型显微硬度计测量试样截面的硬度, 试验载荷为 500 g, 作用时间为 15 s, 沿涂层顶部向下测量, 每个高度测量 4 个点后取平均

值, 消除误差, 每点间距 100  $\mu\text{m}$ 。使用 GF-I 型往复摩擦磨损试验机测量高熵合金涂层的耐磨性, 采用直径为 4 mm 的 Si<sub>3</sub>N<sub>4</sub> 磨球, 试验载荷为 10 N, 磨损时间为 30 min。磨损结束后, 使用电子天平称量磨屑质量, 并且对磨痕进行深度测量和 SEM 微观检测, 分析涂层的磨损机制。

2 结果与分析

2.1 宏观形貌

添加超声振动前后涂层的表面形貌如图 3 所示, 每个涂层由 10 道熔覆道组成。添加超声振动前后, 涂层表面均存在黏粉现象。对经过涂层中垂直方向的裂纹进行了统计, 垂直方向的裂纹从数量上得到一定抑制。原始涂层中存在 8 处垂直于熔覆方向的裂纹, 添加超声振动后, 涂层表面垂直于熔覆方向的裂纹数量明显减少。另一方面, 超声振动的添加影响了熔覆道之间的搭接。

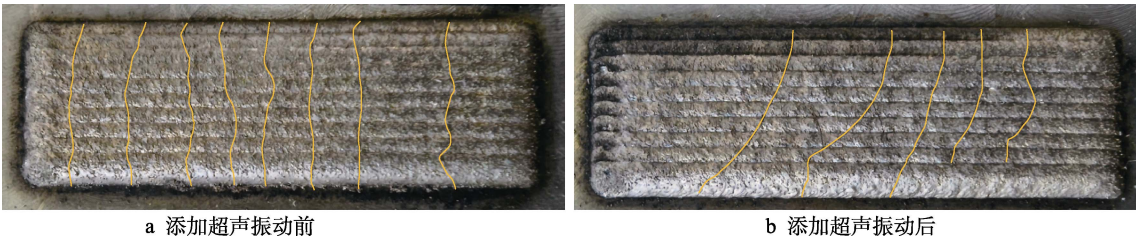


图 3 添加超声振动前后高熵合金涂层表面形貌  
Fig.3 Surface morphology of high-entropy alloy coatings before and after adding ultrasonic vibration:  
a) before adding ultrasonic vibration; b) after adding ultrasonic vibration

涂层的截面形貌如图 4 所示。未添加超声振动时,涂层的致密度较好,无明显气孔,搭接处出现贯穿涂层的裂纹;添加超声振动后,涂层无明显缺陷,搭接处的裂纹消失,熔覆道之间形成良好的冶金结合。在超声振动的作用下,熔池的截面形貌发生变化。原始涂层中,熔池的形貌取决于表面张力与热循环引起的马兰戈尼环流<sup>[24]</sup>,熔池上表面的温度梯度最小,表面张力也最小,熔池轮廓接近圆形,越接近基板,温度梯度越大,熔池的凝固速度也越大,表面张力较小,因此熔池凝固后的形貌为半圆状;添加超声振动后,熔池中的声压梯度产生了声流效应,熔池内部的流动模式发生变化,温度梯度在超声的作用下逐渐减小,熔池的表面张力更加均匀,润湿角减小<sup>[25]</sup>,从而形成椭圆状熔池。

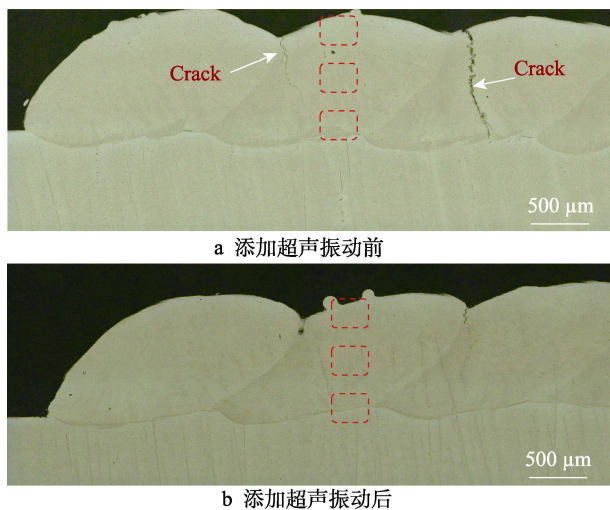


图 4 添加超声前后高熵合金涂层截面形貌  
Fig.4 Cross-sectional morphology of high-entropy alloy coatings before and adding ultrasonic vibration: a) before adding ultrasonic vibration; b) after adding ultrasonic vibration

## 2.2 XRD 物相分析

添加超声振动前后涂层的 XRD 图谱如图 5 所示。经分析可知,加超声前后的涂层均由 FCC 相与 BCC 相组成,与熔覆粉末的物相一致,但涂层中 FCC 的含量在激光熔覆的过程中得到提高。这是由于气雾化制粉的过程中,冷却速度极快 ( $10^5 \sim 10^6$  K/s),粉末内部 FCC 相在 BCC 相内部过度固溶,形成过饱和固溶体,抑制了 FCC 相的偏析;但激光熔覆过程存在重熔的过程,重熔的热量引发过饱和固溶体中亚稳态的 FCC 相重新析出,含量上升<sup>[26]</sup>。AlCoCuFeNi 高熵合金是典型的双相固溶体结构,Al 元素主导 BCC 相,Cu 元素主导 FCC 相。根据金属凝固理论,合金的物相种类由合金中的元素组成决定,物相分布与含量则与合金的凝固过程紧密相关<sup>[27-28]</sup>。超声振动作为一种外部能量场,不会影响涂层内部的物相种类,空化效应与声流效应主要影响高熵合金的熔体流动方式、温

度梯度等。从 XRD 图谱中可知,添加超声振动后,FCC 相的衍射峰强度有明显提高,说明涂层中的 FCC 相含量增加。这是由于超声振动引起声流效应促进了熔池内部的热循环,熔池底部较大的温度梯度得到减缓,成分过冷区域面积增大;另一方面,空化效应可以破坏正在生长的柱状晶,破碎的晶粒可以作为形核的基点<sup>[19]</sup>,温度梯度的降低扩大了固液界面前沿的成分过冷区域,更加有利于等轴晶的形核与长大,Cu 元素主导的 FCC 相则更容易析出。

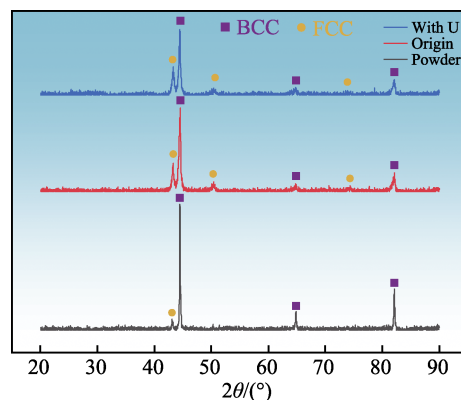


图 5 添加超声振动前后高熵合金涂层 XRD 图谱  
Fig.5 Cross-sectional morphology of high-entropy alloy coatings before and after adding ultrasonic vibration

## 2.3 微观组织

添加超声振动前后涂层不同位置的微观组织形貌如图 6 所示。由于背散射电子模式下 BCC 相与 FCC 相的衬度不同,因此采用背散射电子模式进行拍摄。合金凝固组织的形态与温度梯度 ( $G$ ) 和冷却速度 ( $R$ ) 有着密切的联系<sup>[29]</sup>。原始涂层中,涂层顶部存在大量细小的等轴晶,Cu 元素主导的 FCC 相大量析出,形状呈条带状,基体部分则是 BCC 相。这是由于在 AlCoCuFeNi 高熵合金中,Cu 元素与其他 4 种元素之间有一定的混合焓差异,合金凝固过程中,Cu 元素较难与其他元素形成稳定的键合<sup>[30-32]</sup>,产生了偏析现象;另一方面,Cu 元素的熔点低于 Fe、Co、Ni 等元素,凝固时固相线的移动与溶质再分配造成了 Cu 元素更容易在晶界处偏析。涂层中部的微观组织中,出现了大量的柱状晶,Cu 元素仅在柱状晶内部以斑点的形式偏析,没有出现条带状的大面积偏析。这是因为随着凝固深度的增加,温度梯度迅速增大,此时的环境更加利于柱状晶的生长,Cu 元素在快速凝固效应的影响下来不及发生偏析。而在涂层底部,温度梯度达到最大,固液界面上凸起的枝晶迅速生长,并且形成二次枝晶臂。

添加超声振动后,涂层顶部依然以细小的等轴晶为主,Cu 元素大量析出。涂层中部的微观组织由柱状晶转变为等轴晶,这是由于超声振动引发的声流效应影响了熔池的流动模式<sup>[19]</sup>,激光产生的热量在声流

效应的搅拌作用下分布得更加均匀,减小了熔池的温度梯度,成分过冷区域的面积增大,为等轴晶的生长提供了良好的环境。涂层底部原本粗大的树枝晶被空化效应产生的微冲击波与瞬时的高温打断<sup>[22]</sup>,合金的形核基点数量大幅上升,形成了更多的等轴晶。

2.4 裂纹抑制

涂层顶部搭接处的 EBSD 相分布如图 7 所示。可以看到,原始涂层的搭接处以 BCC 相为主,仅在裂纹的两侧出现少许 FCC 相。结合 XRD 的数据分析,

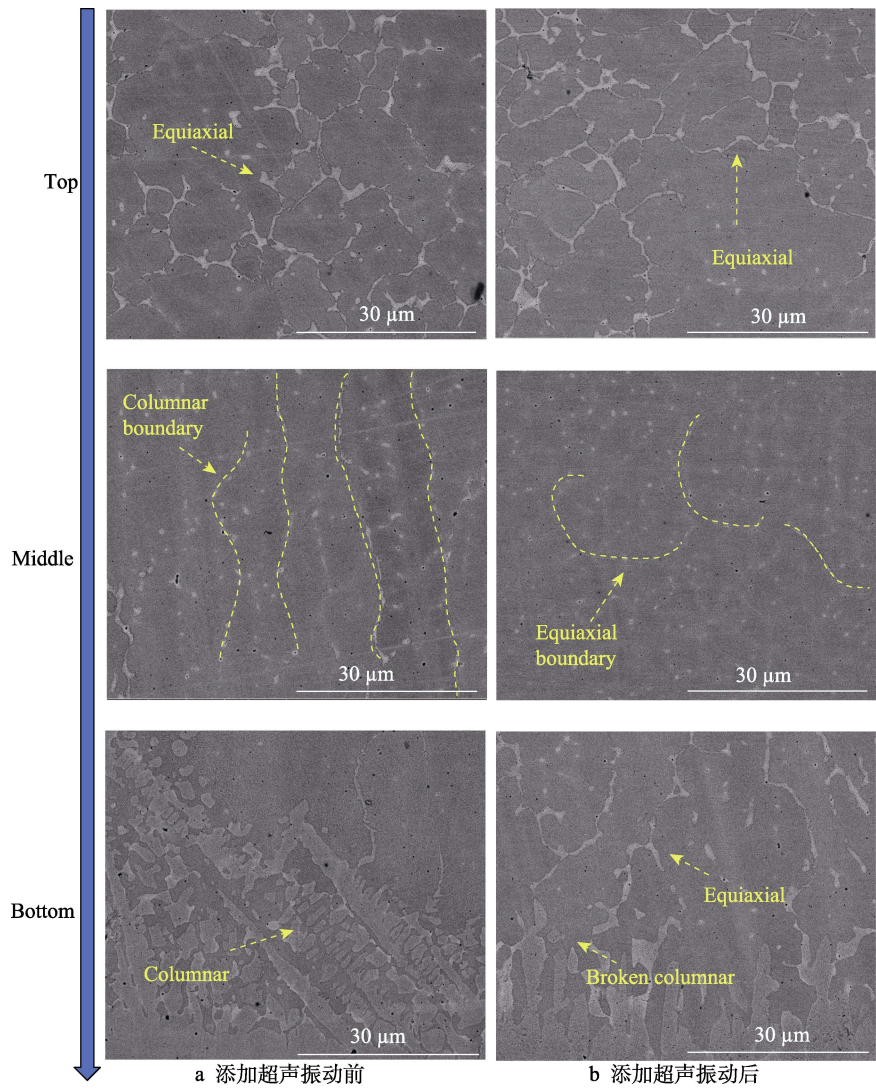


图 6 添加超声前后高熵合金涂层不同位置微观组织的 SEM 形貌  
Fig.6 SEM microstructure of high entropy alloy coatings at different positions before and after adding ultrasonic vibration: a) before adding ultrasonic vibration; b) after adding ultrasonic vibration

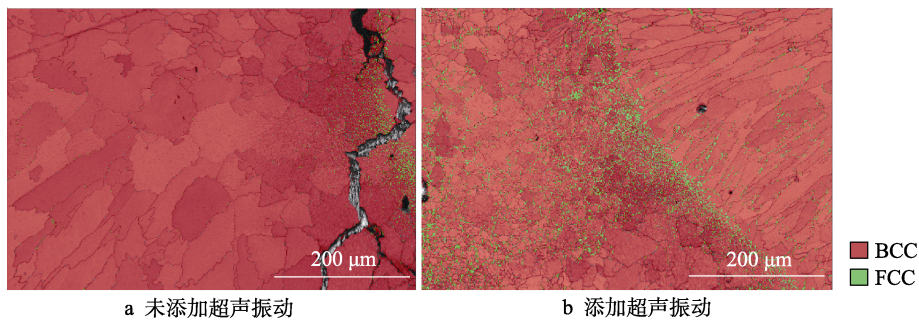


图 7 添加超声前后高熵合金涂层搭接处的相分布  
Fig.7 Phase distribution at the lap of high entropy alloy coating before and after adding ultrasonic vibration: a) before adding ultrasound; b) after adding ultrasonic vibration

由于激光的重熔作用,亚稳态的 FCC 相在重熔过程中重新析出。添加超声振动后,搭接处的晶粒被大幅细化,并没有看到沿搭接处扩展的裂纹。FCC 相在晶界处大量偏析,这些晶界处的 FCC 相有利于抑制裂纹的扩展。

本次试验的原始样品在搭接处出现了贯穿涂层的裂纹,裂纹源的微观组织如图 8 所示。激光热源的能量密度极高,熔池的冷却速度可达  $10^8$  K/s 以上,熔覆层局部的快热快冷将产生残余应力,当残余应力积累至一定数量时,合金内部的冶金结合力不足以对抗残余应力,进而产生开裂,影响涂层的整体力学性能<sup>[33]</sup>。研究人员通过数值模拟对激光熔覆过程中的残余应力进行了研究,发现熔覆道搭接处的横向残余应力数值较大,这可能是由于搭接处受到激光的二次加热,过量的热输入打破了原有的热应力平衡,产生了更多的残余应力<sup>[34]</sup>。从裂纹处的微观组织可以看到,裂纹通过晶界向涂层内部扩展。原始涂层的搭接处晶粒较大,晶界宽度较小;添加超声振动后,搭接处的晶粒明显得到细化,晶界数量增加,且晶界宽度增加,

搭接处起始的裂纹宽度减小,晶界析出相抑制了裂纹的进一步扩展。

从图 8 裂纹处的元素分布情况可以判断,原始涂层搭接处,Al、Co、Fe、Ni 等 4 种元素分布均匀,Cu 元素的偏析呈斑点状,且并未聚集在晶界处。添加超声振动后,Co、Fe、Ni 等 3 种元素分布均匀,Al 元素在晶粒内部偏聚,Cu 元素在晶界处大量偏析,呈向“网状”结构。检测区域的元素含量如表 3 所示,可以发现,Cu 元素的含量上升。Cu 元素主导的 FCC 相具有更多的滑移系,在微观应力传播的过程中,有利于吸收大量的应力<sup>[35]</sup>;Al 元素主导的 BCC 相的滑移系相对较少,吸收应力的能力较差,因此更容易积累残余应力,导致开裂。AlCoCuFeNi 高熵合金在凝固过程中,Cu 元素的熔点较低,且与其他元素存在较大的混合焓差异,导致凝固时 Cu 元素在晶界处偏析,产生液膜。超声振动可以细化涂层晶粒,减小局部的温度梯度,进而促进 FCC 相在晶界处的偏析,晶界处的液膜宽度增加,从而阻碍裂纹的扩展,高熵合金涂层的连续性提升。

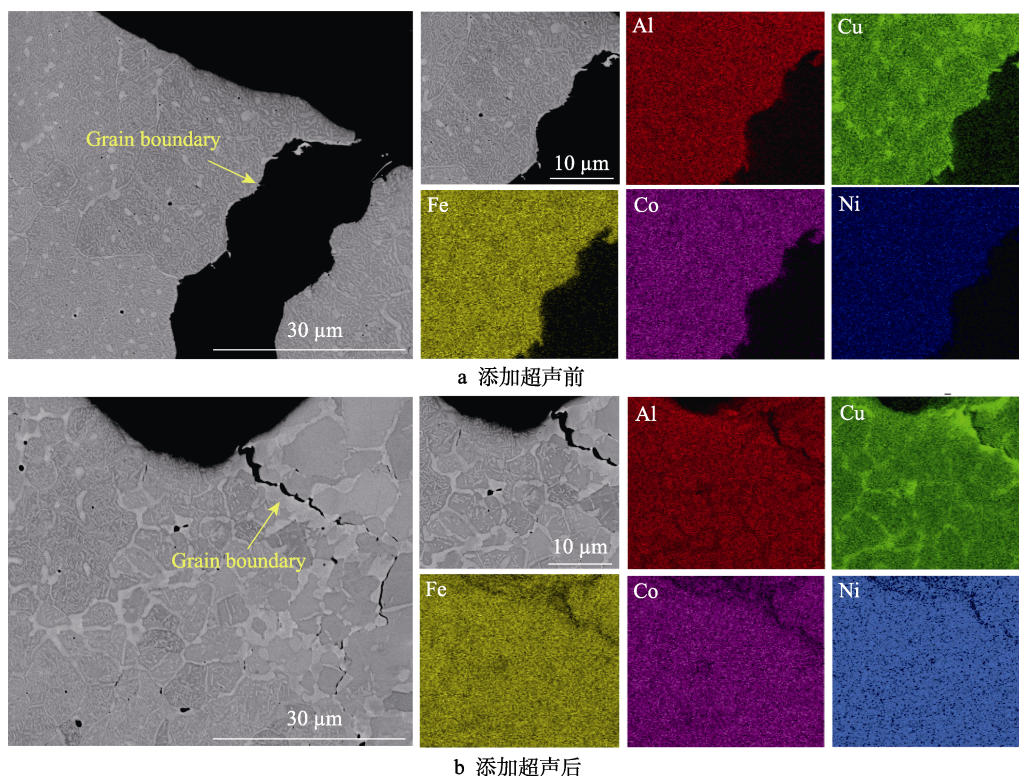


图 8 添加超声振动前后涂层裂纹处的微观形貌 SEM 与元素分布 EDS

Fig.8 Microscopic morphology and elemental distribution at coating cracks before and after adding ultrasonic vibration: a) before adding ultrasonic vibration; b) after adding ultrasonic vibration

表 3 添加超声振动前后裂纹区域元素含量  
Tab.3 Elemental content of cracked area before  
and after adding ultrasonic vibration

	Al	Cu	Fe	Co	Ni
Sample					at. %
Origin	18.6	25.4	20.7	18.0	17.2
With U	18.8	28.0	17.2	17.2	17.3

## 2.5 显微硬度

添加超声前后涂层深度方向的显微硬度变化曲线如图 9 所示。结果表明,未添加超声振动的涂层平均硬度为 503HV0.5,添加超声振动后,涂层的平均显微硬度提升至 526HV0.5。合金的硬度符合 Hall-Petch 关系,当晶粒细化后,晶界的数量急剧上

升,需要更大的外力打破晶界处的位错堆积与应力集中,因此合金的强度提升<sup>[36]</sup>。所超声振动改变了涂层的截面形貌,熔高减小。添加超声振动后涂层顶部的硬度略小于原始涂层,这是因为涂层顶部晶粒的显著细化,产生了大量 Cu 元素主导的 FCC 软相,使得表面硬度有所下降。另一方面,从图 9 中还能看到,原始涂层存在明显的过渡区,这是由于基板的稀释效应导致涂层下部的元素成分变化,硬度下降;添加超声后,过渡区面积减小,涂层与基板之间有很明显的硬度变化,符合高硬度低稀释率的涂层要求。

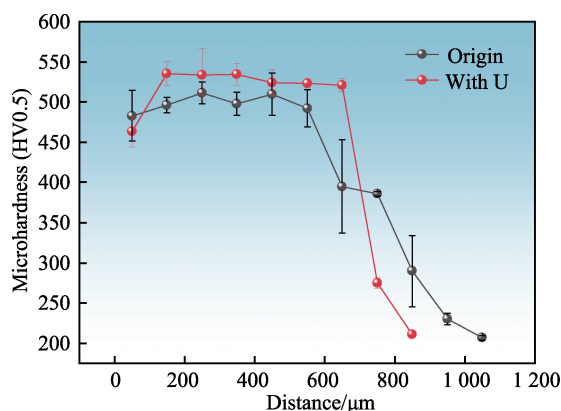


图 9 添加超声振动前后涂层显微硬度  
Fig.9 Microhardness of coatings before and after adding ultrasonic vibration

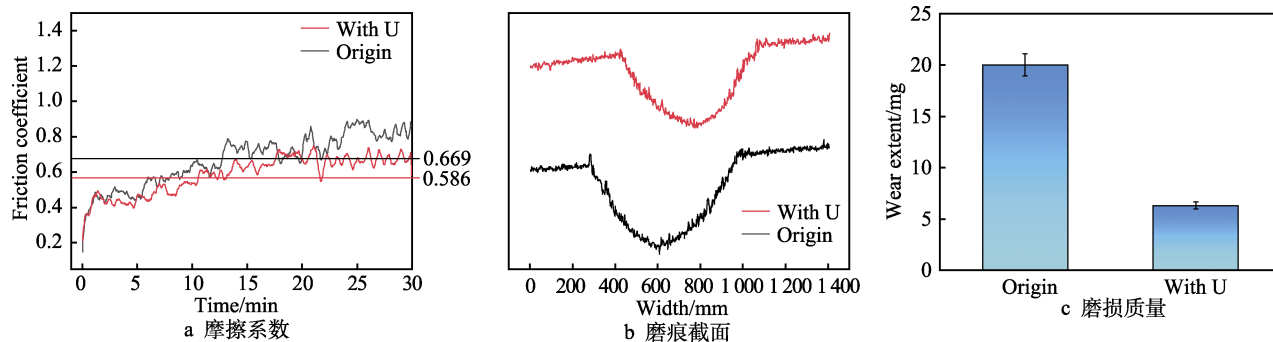


图 10 添加超声振动前后涂层摩擦性能变化

Fig.10 Changes in coating friction properties before and after adding ultrasonic vibration: a) friction coefficient; b) wear scar section; c) wear mass

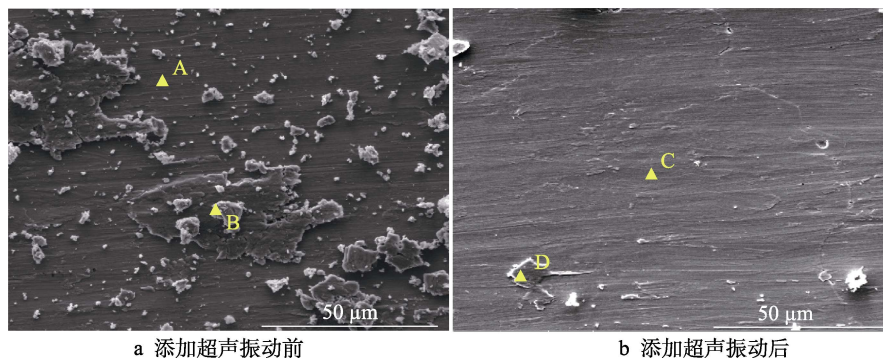


图 11 添加超声振动前后涂层磨痕的微观形貌

Fig.11 Microscopic morphology of coating abrasions before and after adding ultrasonic vibration: a) before adding ultrasonic vibration; b) after adding ultrasonic vibration

## 2.6 室温摩擦性能

涂层摩擦因数曲线、磨损量与磨痕截面如图 10 所示。可以看出,原始涂层的摩擦过程处于不稳定状态,随着摩擦时间的延长,摩擦因数逐渐上升;添加超声振动后,摩擦因数明显降低,曲线上升缓慢,平均摩擦因数由 0.669 减小至 0.586。从磨痕截面可以看出,添加超声振动后,涂层的磨痕深度减小,由 62.5  $\mu\text{m}$  减小至 50.4  $\mu\text{m}$ ,磨损量也由 20.1 mg 减小至 6.9 mg。在双相高熵合金的磨损过程中, BCC 相可以避免大面积的磨料磨损, FCC 相可以抑制磨损过程中的裂纹扩展。添加超声振动后,涂层的摩擦性能提升,这可能是由于超声振动引发的 FCC 析出相改变了原始合金中的 BCC 相与 FCC 相的配比,达到了更加耐磨的比例。

为了进一步研究超声振动提升涂层耐磨性能的机制,观察了磨痕的微观形貌,如图 11 所示。结果表明,原始涂层的磨痕不存在微裂纹,磨痕的形状为平行于磨球滑动方向的多道沟槽,同时表面存留大块黏连的磨屑。由此可以判断,原始涂层的磨损机制为磨粒磨损<sup>[37]</sup>,摩擦引起的微裂纹贯穿了 BCC 基体,粗大的晶粒不利于微裂纹的消失,产生大量的未脱落磨屑。添加超声振动后,磨痕表面同样存在平行的沟槽,磨损机制仍然为磨粒磨损,但是磨痕表面较为整洁,无明显黏连的磨屑。对磨痕基体与磨屑进行了 EDS 元素扫描,如图 12 所示。发现磨屑中氧元素的

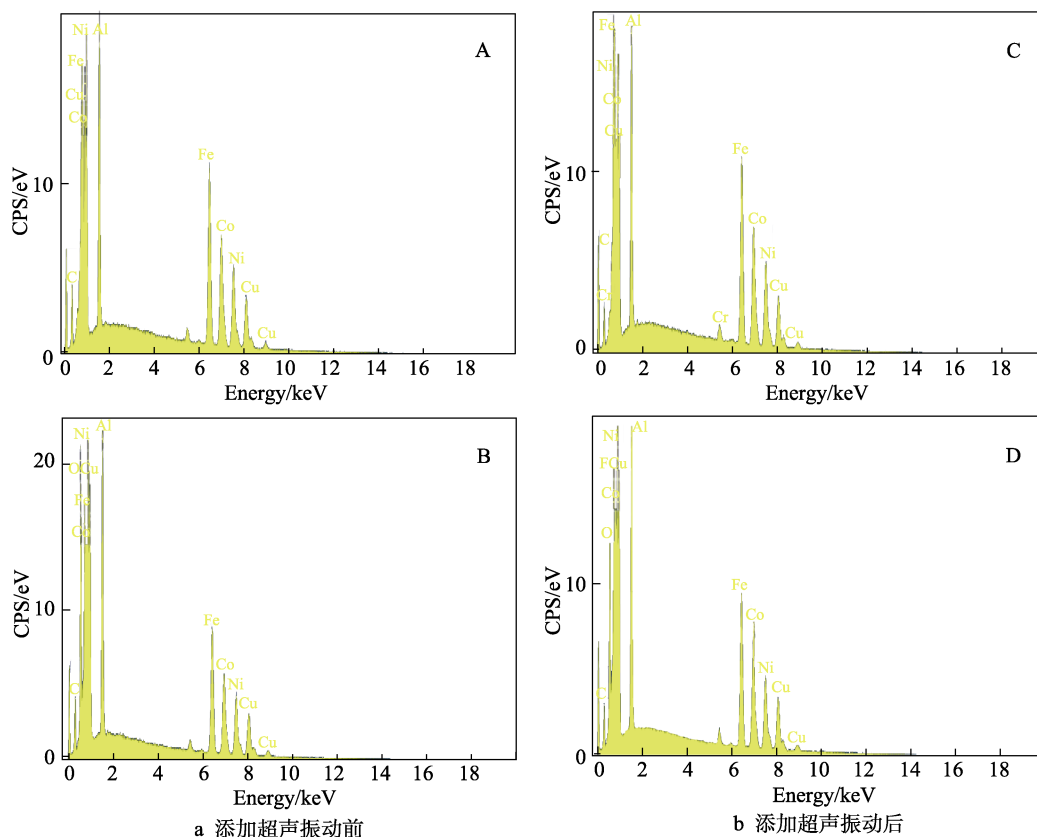


图 12 添加超声振动前后涂层磨损元素含量图谱

Fig.12 Mapping of elemental content in coating abrasions before and after adding ultrasonic vibration: a) before adding ultrasonic vibration; b) after adding ultrasonic vibration

峰值较高, 磨损基体中不存在氧元素, 因此磨损过程中包含着轻微的氧化磨损机制。由此可知, 高熵合金涂层的磨损机制为磨粒磨损与轻微的氧化磨损, 添加超声振动后, 涂层耐磨性能的提升得益于晶粒的细化。

### 3 结论

本文在激光熔覆 AlCoCuFeNi 高熵合金涂层的过程中, 采用自主设计的实验平台, 添加了底部超声振动, 对比了超声振动添加前后涂层的宏观形貌、物相组成、微观组织与晶粒形态的变化, 研究了超声振动对高熵合金涂层显微硬度与室温摩擦性能的调控机制, 得出如下主要结论:

1) 超声振动作用下, 涂层的宏观形貌发生变化, 高频振动减小了熔池与基板的接触角, 涂层截面由半圆状变为椭圆状。原始涂层中, 搭接处存在贯穿涂层的裂纹; 添加超声振动后, 涂层连续性好, 搭接处形成良好的冶金结合。

2) 超声振动产生的声流效应改变了熔池的流动模式, 搅拌作用使得温度梯度减小, 涂层中密集的树枝晶被抑制。空化效应产生的微冲击波与瞬时高温打断了涂层内部的柱状晶, 破碎的柱状晶增加了凝固晶核的数量, 晶粒细化显著。熔池温度梯度的变化与晶

粒细化增加了 FCC 相的析出, 在涂层搭接处以“网状”形式分布, 抑制了裂纹的扩展。

3) 超声振动作用下, 涂层的力学性能得到提升。平均显微硬度由 503HV0.5 提升至 526HV0.5。涂层的摩擦因数减小, 曲线波动幅度减小, 摩擦因数由 0.669 减小至 0.586。超声振动引起的 FCC 析出相减少了涂层摩擦过程中的微裂纹, 晶粒的细化提升了涂层的磨损性能, 磨损机制未发生变化, 均为磨粒磨损与轻微氧化磨损。

### 参考文献:

- [1] CANTOR B, CHANG I T H, KNIGHT P, et al. Microstructural Development in Equiatomic Multicomponent Alloys[J]. Materials Science and Engineering: A, 2004, 375: 213-218.
- [2] YE H J W, CHEN S K, LIN S J, et al. Nanostructured High-Entropy Alloys with Multiple Principal Elements: Novel Alloy Design Concepts and Outcomes[J]. Advanced Engineering Materials, 2004, 6(5): 299-303.
- [3] BORKAR T, GWALANI B, CHOUDHURI D, et al. A Combinatorial Assessment of  $Al_xCrCuFeNi_2$  ( $0 < x < 1.5$ ) Complex Concentrated Alloys: Microstructure, Microhardness, and Magnetic Properties[J]. Acta Materialia,

- 2016, 116: 63-76.
- [4] MIRACLE D, MILLER J, SENKOV O, et al. Exploration and Development of High Entropy Alloys for Structural Applications[J]. *Entropy*, 2014, 16(1): 494-525.
- [5] CHO F Y, TUNG S W, OUYANG F Y. High Temperature Oxidation Behavior of High Entropy Alloy  $\text{Al}_4\text{Co}_3\text{Cr}_{25}\text{Cu}_{10}\text{Fe}_{25}\text{Ni}_{33}$  in Oxygen-Containing Atmospheres[J]. *Materials Chemistry and Physics*, 2022, 278: 125678.
- [6] OH S H, LEE K, LEE J. The Gaps between Knowing and Doing in Hearing Aid Fitting Management[J]. *Journal of Audiology and Otology*, 2017, 21(2): 120-123.
- [7] YU Y, WANG J, LI J S, et al. Tribological Behavior of  $\text{AlCoCrCuFeNi}$  and  $\text{AlCoCrFeNiTi}_{0.5}$  High Entropy Alloys under Hydrogen Peroxide Solution Against Different Counterparts[J]. *Tribology International*, 2015, 92: 203-210.
- [8] ZHOU E Z, QIAO D X, YANG Y, et al. A Novel Cu-Bearing High-Entropy Alloy with Significant Antibacterial Behavior Against Corrosive Marine Biofilms[J]. *Journal of Materials Science & Technology*, 2020, 46: 201-210.
- [9] BRAECKMAN B R, BOYDENS F, HIDALGO H, et al. High Entropy Alloy Thin Films Deposited by Magnetron Sputtering of Powder Targets[J]. *Thin Solid Films*, 2015, 580: 71-76.
- [10] ALIYU A, SRIVASTAVA C. Microstructure and Corrosion Performance of  $\text{AlFeCoNiCu}$  High Entropy Alloy Coatings by Addition of Graphene Oxide[J]. *Materialia*, 2019, 8: 100459.
- [11] GAO P H, FU R T, CHEN B Y, et al. Corrosion Resistance of  $\text{CoCrFeNiMn}$  High Entropy Alloy Coating Prepared through Plasma Transfer Arc Claddings[J]. *Metals*, 2021, 11(11): 1876.
- [12] ZHANG M N, ZHOU X L, WANG D F, et al.  $\text{AlCoCuFeNi}$  High-Entropy Alloy with Tailored Microstructure and Outstanding Compressive Properties Fabricated via Selective Laser Melting with Heat Treatment[J]. *Materials Science and Engineering: A*, 2019, 743: 773-784.
- [13] ARIF Z U, KHALID M Y, UR REHMAN E, et al. A Review on Laser Cladding of High-Entropy Alloys, Their Recent Trends and Potential Applications[J]. *Journal of Manufacturing Processes*, 2021, 68: 225-273.
- [14] WANG Y, LI R D, NIU P D, et al. Microstructures and Properties of Equimolar  $\text{AlCoCrCuFeNi}$  High-Entropy Alloy Additively Manufactured by Selective Laser Melting[J]. *Intermetallics*, 2020, 120: 106746.
- [15] WANG J W, ZHANG M L, WANG H M, et al. Mitigating Hot-Cracking of Laser Melted  $\text{CoCrFeNiMnTi}_x$  High-Entropy Alloys[J]. *Materials Letters*, 2022, 314: 131771.
- [16] TODARO C J, EASTON M A, QIU D, et al. Grain Structure Control during Metal 3D Printing by High-Intensity Ultrasound[J]. *Nature Communications*, 2020, 11(1): 142.
- [17] WANG X H, LIU S S, ZHAO G L, et al. In-Situ Formation Ceramic Particles Reinforced Fe-Based Composite Coatings Produced by Ultrasonic Assisted Laser Melting Deposition Processing[J]. *Optics & Laser Technology*, 2021, 136: 106746.
- [18] YANG Z C, WANG S H, ZHU L D, et al. Manipulating Molten Pool Dynamics during Metal 3D Printing by Ultrasound[J]. *Applied Physics Reviews*, 2022, 9(2): 021416.
- [19] WEI X, LI X L, ZHANG L Q, et al. Effect of In-Situ Ultrasonic Impact Treatment on Flow and Solidification Behavior of Laser Metal Deposition: By Finite Element Simulation[J]. *International Journal of Heat and Mass Transfer*, 2022, 192: 122914.
- [20] ZHANG Z, LI J N, ZHAO B B, et al. Microstructure and Excellent Performance Enhancement of MEA Base Composites with Multi-Phase Induced by Ultrasonic Assisted Laser Technology[J]. *Journal of Alloys and Compounds*, 2023, 938: 168639.
- [21] HAN X, LI C, YANG Y P, et al. Experimental Research on the Influence of Ultrasonic Vibrations on the Laser Cladding Process of a Disc Laser[J]. *Surface and Coatings Technology*, 2021, 406: 126750.
- [22] WANG B, TAN D Y, LEE T L, et al. Ultrafast Synchrotron X-Ray Imaging Studies of Microstructure Fragmentation in Solidification under Ultrasound[J]. *Acta Materialia*, 2018, 144: 505-515.
- [23] JI F L, QIN X P, HU Z Q, et al. Influence of Ultrasonic Vibration on Molten Pool Behavior and Deposition Layer Forming Morphology for Wire and Arc Additive Manufacturing[J]. *International Communications in Heat and Mass Transfer*, 2022, 130: 105789.
- [24] YANG J, SCHLENGER L M, NASAB M H, et al. Experimental Quantification of Inward Marangoni Convection and Its Impact on Keyhole Threshold in Laser Powder Bed Fusion of Stainless Steel[J]. *Additive Manufacturing*, 2024, 84: 104092.
- [25] 姚喆赫, 沈奇艳, 葛宏江, 等. 超声对激光熔覆成形中熔池润湿行为的影响研究[J]. *表面技术*, 2022, 51(10): 20-29.
- YAO Z H, SHEN Q Y, GE H J, et al. Influence of Ultrasound on the Wetting Behavior of Molten Pool in Laser Cladding[J]. *Surface Technology*, 2022, 51(10): 20-29.
- [26] ZHANG M N, ZHOU X L, WANG D F, et al. Additive Manufacturing of In-Situ Strengthened Dual-Phase  $\text{AlCoCuFeNi}$  High-Entropy Alloy by Selective Electron Beam Melting[J]. *Journal of Alloys and Compounds*, 2022, 893: 162259.
- [27] 范金辉, 翟启杰. 物理场对金属凝固组织的影响[J]. *中国有色金属学报*, 2002, 12(S1): 11-17.
- FAN J H, ZHAI Q J. Effects of Physical Fields on Solidification Structure of Metals[J]. *The Chinese Journal of Nonferrous Metals*, 2002, 12(S1): 11-17.
- [28] 司玉锋, 孟丽华, 陈玉勇.  $\text{Ti}_2\text{AlNb}$  基合金的研究进展[J]. *宇航材料工艺*, 2006, 36(3): 10-13.
- SI Y F, MENG L H, CHEN Y Y. Research Development of  $\text{Ti}_2\text{AlNb}$ -Based Alloy[J]. *Aerospace Materials & Tech-*

- nology, 2006, 36(3): 10-13.
- [29] LI H G, HUANG Y J, JIANG S S, et al. Columnar to Equiaxed Transition in Additively Manufactured CoCrFe-MnNi High Entropy Alloy[J]. Materials & Design, 2021, 197: 109262.
- [30] HU Q, WANG H L, QIAN L H, et al. Effects of Cu Additions on Microstructure and Mechanical Properties of As-Cast CrFeCoNiCu x High-Entropy Alloy[J]. Transactions of Nonferrous Metals Society of China, 2023, 33(6): 1803-1813.
- [31] SONG Y P, YAN L C, PANG X L, et al. Effects of Co-Alloying Al and Cu on the Corrosion Behavior and Mechanical Properties of Nanocrystalline FeCrNiCo High Entropy Alloys[J]. Corrosion Science, 2023, 213: 110983.
- [32] XU M Q, HAN L, SHEN C L, et al. Impact of 3d TM Elements on Cu Segregation in CrCuTiV-Based High Entropy Alloys and Their Mechanical Properties[J]. Vacuum, 2024, 219: 112723.
- [33] SUÁREZ A, AMADO J M, TOBAR M J, et al. Study of Residual Stresses Generated Inside Laser Cladded Plates Using FEM and Diffraction of Synchrotron Radiation[J]. Surface and Coatings Technology, 2010, 204(12/13): 1983-1988.
- [34] YAO M P, KONG F R, TONG W. A 3D Finite Element Analysis of Thermally Induced Residual Stress Distribution in Stainless Steel Coatings on a Mild Steel by Laser Hot Wire Cladding[J]. The International Journal of Advanced Manufacturing Technology, 2023, 126(1): 759-776.
- [35] BEDNARCZYK W, WĄTROBA M, JAIN M, et al. Determination of Critical Resolved Shear Stresses Associated with Slips in Pure Zn and Zn-Ag Alloys via Micro-Pillar Compression[J]. Materials & Design, 2023, 229: 111897.
- [36] HENAGER C H. Reversing Inverse Hall-Petch and Direct Computation of Hall-Petch Coefficients[J]. Acta Materialia, 2024, 265: 119627.
- [37] GUAN Y J, CUI X F, CHEN D, et al. Microstructure and Properties Analysis of FeCoNiAlCu Dual-Phase High-Entropy Alloy Coating by Laser Cladding[J]. Surface and Coatings Technology, 2023, 467: 129695.
- 
- ( 上接第 12 页 )
- [64] PETZOLDT S, REIF J, MATTHIAS E. Laser Plasma Threshold of Metals[J]. Applied Surface Science, 1996, 96: 199-204.
- [65] SOHN H, LIU P P, YOON H, et al. Real-Time Porosity Reduction during Metal Directed Energy Deposition Using a Pulse Laser[J]. Journal of Materials Science & Technology, 2022, 116: 214-223.
- [66] CHEN D, CAI Y H, LUO Y, et al. Analysis on the Microstructure Regulation Based on the Pulsed Laser Oscillating Molten Pool in Laser-PTA Additive Manufacturing[J]. Journal of Manufacturing Processes, 2020, 59: 587-594.
- [67] 范思远, 毛家智, 谢颂伟, 等. 脉冲/连续双光束复合激光熔覆对 316L 不锈钢熔覆组织的影响[J]. 中国激光, 2023, 50(4): 3788/CJL220745.
- FAN S Y, MAO J Z, XIE S W, et al. Effect of Pulsed/Continuous Double-Beam Hybrid Laser Cladding on Microstructure of 316L Stainless Steel[J]. Chinese Journal of Lasers, 2023, 50(4): 3788/CJL220745.
- [68] LU H, ZHANG X H, LIU J, et al. Study on Laser Shock Modulation of Melt Pool in Laser Additive Manufacturing of FeCoCrNi High-Entropy Alloys[J]. Journal of Alloys and Compounds, 2022, 925: 166720.
- [69] LU H, HE Y, ZHAO Z, et al. Strengthening CoCrFeNi High Entropy Alloys via Additive Manufacturing with Laser Shock Modulation of Melt Pool[J]. Materials Science and Engineering: A, 2022, 860: 144295.
- [70] 彭旭, 李斌, 王顺尧, 等. 激波冲击作用下液膜破碎的气液两相流[J]. 物理学报, 2020, 69(24): 209-217.
- PENG X, LI B, WANG S Y, et al. Gas-Liquid Two-Phase Flow of Liquid Film Breaking Process under Shock Wave[J]. Acta Physica Sinica, 2020, 69(24): 209-217.